The Clementine Mission to the Moon: Scientific Overview

Stewart Nozette, P. Rustan, L. P. Pleasance, D. M. Horan, P. Regeon, E. M. Shoemaker, P. D. Spudis, C. H. Acton, D. N. Baker, J. E. Blamont, B. J. Buratti, M. P. Corson, M. E. Davies, T. C. Duxbury, E. M. Eliason, B. M. Jakosky, J. F. Kordas, I. T. Lewis, C. L. Lichtenberg, P. G. Lucey, E. Malaret, M. A. Massie, J. H. Resnick, C. J. Rollins, H. S. Park, A. S. McEwen, R. E. Priest, C. M. Pieters, R. A. Reisse, M. S. Robinson, R. A. Simpson, D. E. Smith, T. C. Sorenson, R. W. Vorder Breugge, M. T. Zuber

In the course of 71 days in lunar orbit, from 19 February to 3 May 1994, the Clementine spacecraft acquired just under two million digital images of the moon at visible and infrared wavelengths. These data are enabling the global mapping of the rock types of the lunar crust and the first detailed investigation of the geology of the lunar polar regions and the lunar far side. In addition, laser-ranging measurements provided the first view of the global topographic figure of the moon. The topography of many ancient impact basins has been measured, and a global map of the thickness of the lunar crust has been derived from the topography and gravity.

In early 1992, after a 4-month effort by the National Aeronautics and Space Administration (NASA), the U.S. Department of Defense, and industry, it was concluded that a mission to a near-Earth asteroid using new lightweight technology was desirable and feasible. The mission was subsequently expanded by 2 months to include mapping of the moon to demonstrate spacecraft and sensor performance before the demanding asteroid flyby. The interstage adapter of the spacecraft, which houses the solid rocket motor, was designed to remain in a highly eccentric Earth orbit as a radiation experiment platform and additional sensor target. The name Clementine was selected for the spacecraft because the old ballad "My Darlin' Clementine" is about the daughter of a miner and this mission would assist in determining the mineral content of the moon and the asteroid. And, as in the song, after the asteroid flyby, Clementine was to be "lost and gone forever." The Clementine spacecraft was built at the Naval Research Laboratory in Washington, D.C., and carried sensors designed and built by the Lawrence Livermore National Laboratory.

The spacecraft was launched with a refurbished Titan IIG ICBM into a 226-km by 259-km parking orbit at a 67° inclination on 25 January 1994. On 3 February, the spacecraft was spun to 60 revolutions per minute, and the kick motor was fired, injecting the spacecraft into a phasing orbit transfer trajectory to the moon. The spacecraft was placed into a 400-km by 2940-km, 5-hour orbit around the moon on 19 February, where it remained until 3 May. The asteroid flyby was aborted on 7 May 1994 because a software error had depleted the spacecraft attitude-control propellant.

The spacecraft is an octagonal prism about 2 m high (Fig. 1). A 110-pound thruster for maneuvers in space is on one end of the prism, and a high-gain fixed dish antenna is on the other end. The power system consists of a gimbaled, single-axis, GaAs-Ge solar array, which provides a total spacecraft power of 360 W at 30 V dc, with a specific power of 240 W/kg, based on the lightweight construction. The spacecraft dry mass is about 227 kg, with a roughly equal mass for liquid fuel.

The main instrumentation on Clementine consists of four cameras, one of which is equipped with a laser-ranging system (Fig. 2 and Table 1). The cameras include an ultraviolet-visible (UVVIS) camera, a long-wave infrared (LWIR) camera, the laser-ranger (LIDAR) high-resolution (HIRES) camera, and a near-infrared (NIR) camera. The fields of view of these cameras are shown in Fig. 2. The spacecraft also has two star-tracker cameras, used mainly for attitude determination, but they also serve as wide-field cameras for various scientific and operational purposes. Tracking data from the spacecraft's S-band transponder provided information on the lunar gravity field. The sensors are all located on one side, 90° away from the solar panels. Clementine has 12 small attitude-control jets that were used to orient the spacecraft to point the cameras to desired targets. The attitude-control system includes the two star-tracker cameras and two lightweight inertial measurement units, based on a ring laser gyro and an interferometric fiber optic gyro. During initial deployment at low Earth orbit, the spacecraft was stabilized on all three of its axes. The spacecraft was then three-axis–stabilized in lunar orbit by means of reaction wheels, with a precision of 0.05° in control and 0.03° in knowledge. The spacecraft data processing was performed by three computing systems (*1*).

The UVVIS camera has a catadioptric telescope with fused silica lenses focused onto a coated Thomson charge-coupled device (CCD) imager. Active wavelength response is limited on the short wavelength end by the transmission of fused silica and by the optical blur of the lens, and on the long end by the response of the CCD. Five

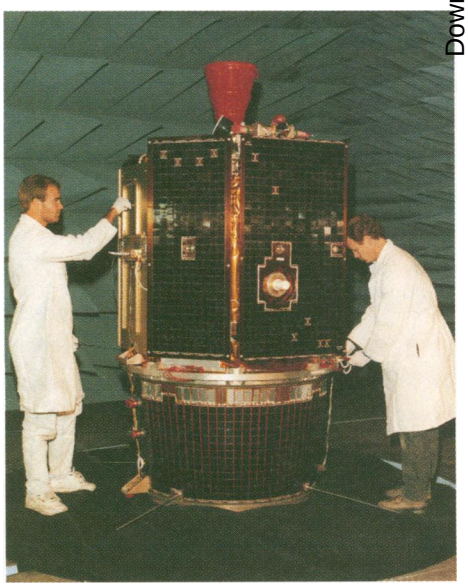

Fig. 1. The spacecraft, on top of its adapter, being prepared for testing at the Naval Research Laboratory's anechoic chamber.

S. Nozette and P. Rustan, Ballistic Missile Defense Organization, Washington, DC 22314. L. P. Pleasance, J. F. Kordas, I. T. Lewis, H. S. Park, R. E. Priest, Lawrence Livermore National Laboratory, Livermore, CA 94550. D. M. Horan, P. Regeon, C. L. Lichtenberg, Naval Research Laboratory, Washington, DC 20375. E. M. Shoemaker, E. M. Eliason, A. S. McEwen, M. S. Robinson, U.S. Geological Survey, Flagstaff, AZ 86001. P. D. Spudis, Lunar and Planetary Institute, Houston, TX 77058. C. H. Acton, B. J. Buratti, T. C. Duxbury, Jet Propulsion Laboratory, Pasadena, CA 91109. D. N. Baker and B. M. Jakosky, LASP, University of Colorado, Boulder, CO 80309. J. E. Blamont, Centre National d'Etudes Spatiales, Paris, France. M. P. Corson, J. H. Resnick, C. J. Rollins, Research Support Instruments, Alexandria, VA 22314. M. E. Davies, Rand Corporation, Santa Monica, CA 90407. P. G. Lucey, University of Hawaii at Manoa, Honolulu, HI 96822. E. Malaret, Applied Coherent Technology, Herndon, VA 22070. M. A. Massie, Pacific Advanced Technology, Solvang, CA 94550. C. M. Pieters, Brown University, Providence, RI 02912. R. A. Reisse, Science Inquiries, Catonsville, MD 21228. R. A. Simpson, Stanford University, Stanford, CA 94305. D. E. Smith, Goddard Space Flight Center, Greenbelt, MD 20771. T. C. Sorenson, Allied Signal, Alexandria, VA 22314. R. W. Vorder Breugge, Science Applications International, Washington, DC 20024. M. T. Zuber, Johns Hopkins University, Baltimore, MD 21218.

spectral bands and one broad band (Fig. 3) can be selected from a filter wheel. The CCD is a frame-transfer device, accomplishing electronic shuttering by rapidly shifting the active pixel area into the storage area, pausing for the integration time, then rapidly shifting the captured image into a storage buffer, from which the image is read. The CCD electronics allow three gain states. With the day side of the moon as a target, typical integration times were as short as several milliseconds in the lowest gain state (1000 electrons per bit) near subsolar illumination points at the brighter spectral bands, increasing to 40 ms near the polar regions in the middle gain setting for the weaker 415- and 1000-nm spectral bands.

The HIRES camera combines a lightweight telescope with an image intensifier coupled with a frame-transfer CCD imager. Spectral response is from 0.4 to 0.8 μm. Five spectral bands are selectable from a filter wheel; a sixth filter position is opaque, to protect the image intensifier. Images of the day side of the moon used intensifier gate times on the order of 1 ms with low gain settings. Lifetime concerns about the photocathode and microchannel plates in the intensifier unit drove operational settings to low exposures. This resulted in photon shot noise significantly contributing to the overall noise in the HIRES sensor.

The LIDAR unit shares the telescope of the HIRES camera, splitting the 1064-nm return signal from the Nd–yttrium-aluminum-garnet (YAG) source off to an avalanche photodiode detector (APD) with a dichroic filter. The optics are nonimaging, providing an exit pupil through simple relay optics at the APD. Range is determined by the number of clock cycles between the laser start pulse and the received signal. The clock counter has only 14 bits, owing to hardware availability limitations. In order to allow returns up to the 640-km maximum range required in the lunar mission, we binned four returns to a clock count, turning the 23-MHz response into a 39.972-m bin. Internal memory in the LIDAR unit saves up to six "returns" per laser firing, with up to four saved in the programmable search range. Threshold is set for the best compromise between missed detections and false alarms.

The NIR camera uses a catadioptric lens with a 256 by 256 pixel InSb focal plane array (FPA) mechanically cooled to cryogenic temperature. The FPA operated at 70 ± 0.5 K at the moon. Six wavebands were available (Fig. 3).

The LWIR camera uses a catadioptric lens with a 128 × 128 HgCdTe FPA. The FPA was operated at 65 K. Wavelength range was controlled by the cold filter to 8.0 to 9.5 μm.

The wide field of view star-tracker cameras have a concentric optics design with a fiber optic field flattener to couple the image surface to a CCD array. The primary function of the star-tracker cameras was to provide stellar images that were processed against an on-board star catalog to establish absolute angular references for navigation. The scientific uses of the cameras were secondary. Only broadband operation was available. The line-transfer electronic shuttering limited imaging to dim targets such as the lunar surface illuminated by earthshine.

Extensive preflight calibration, acquired with an automated calibration facility at Lawrence Livermore National Laboratory, attempted to cover light levels similar to those expected from the lunar surface and to span the camera settings required for lunar mapping. The measurements included radiometric sensitivity; FPA uniformity; gain and offset scale factors; temporal-spatial noise; dark-noise dependence on FPA temperatures, integration times or input voltage levels, and spectral response of FPA; optical distortion map; point-spread function; and electronic warm-up time and cryocooler cool-down time. For the thermally sensitive sensors such as the LWIR camera, the noise measurement was performed in a vacuum chamber to simulate the space thermal environment.

Many preflight calibration coefficients were applied to lunar data showing reasonable agreement with expected performance. In-flight calibration data allow corrections such as those for vacuum flight condition and sensor degradation over mission life-

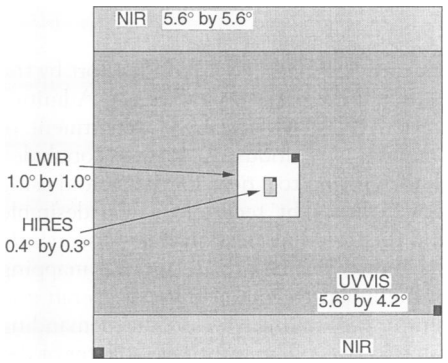

Fig. 2. Fields of view and alignment of the UVVIS, NIR, LWIR, and HIRES cameras. Small black squares show the positions of the initial pixels.

Table 1. Clementine instrument parameters.

	UVVIS	Star tracker	NIR	LWIR	HIRES	LIDAR receiver*	LIDAR transmitter†
Focal plane array	Thomson CCD	Thomson CCD	Amber InSb	Amber HgCdTe	Intensified CCD	SiAPD	
Pixel format	384 × 288	384 × 576	256 × 256	128 × 128	384 × 288	Single cell	
Pixel size (μm)	23 × 23	23 × 23	38 × 38	50 ×50	23 × 23	0.5 mm^2	
Clear aperture (mm)	46	14	29	131	131	Shared with HIRES	38
Focal length (mm)	90	17.5	96	350	1250	Shared with HIRES	99
Array field of view (degrees)	5.6 × 4.2	28 × 43	5.6 × 5.6	1.0 × 1.0	0.4 × 0.3	0.057	
Bandpass filters (μm)	0.415 ± 0.020	0.4 to 1.1	1.10 ± 0.03	8.0 to 9.5	0.415 ± 0.020	0.4 to 1.1	1.064 and 0.532
	0.750 ± 0.005		1.25 ± 0.03		0.560 ± 0.005		
	0.900 ± 0.015		1.50 ± 0.03		0.650 ± 0.005		
	0.950 ± 0.015		2.00 ± 0.03		0.750 ± 0.010		
	1.000 ± 0.015		2.60 ± 0.03		0.4 to 0.8		
	0.4 to 0.95		2.78 ± 0.06				
Integration times (ms)	0.2 to 773	0.2 to 773	11, 33, 57, 95	0.144, 1.15, 2.30, 4.61	0.2 to 773		
Gains	150, 350, and 1000 *e*/bit	75, 150, and 350 *e*/bit	0.5 to 36×	0.5 to 36×	150, 350, and 1000 *e*/bit	100×	
Offsets (bits)	5	5	8	8	5	None	
Power (W)	4.5	4.5	11.0	13.0	9.5	Housed in HIRES	6.8 at 1 Hz; 2.6 quiescent
Weight (g)	410	290	1920	2100	1120	Housed in HIRES	1250

*The A/D resolution of the LIDAR receiver was 14 bits (40 m per bit), whereas all of the cameras had a resolution of 8 bits. †The laser used for the LIDAR was an Nd-YAG that produced a pulse of width <10 ns. At a wavelength of 1.064 μm, it produced a pulse with an energy of 171 mJ and a divergence of <500 μrad. At a wavelength of 0.532 μm, it produced a 9-mJ pulse with a 4-mrad divergence.

time to be added to the preflight calibration results. The combined calibration is expected to be better than 5%.

Over the course of 71 days in lunar orbit, Clementine mapped the 38 million square kilometers of the moon in 11 visible and near-infrared colors (nearly one million images). The spacecraft took 620,000 high-resolution and about 320,000 mid-infrared thermal images, mapped the topography of the moon with the LIDAR, improved our knowledge of the surface gravity field of the moon through radio tracking, and carried a charged-particle telescope to characterize the solar and magnetospheric energetic-particle environment. Most of the sensors on the spacecraft met or exceeded expectations. We have had our first view of the global color of the moon and identified major compositional provinces, studied several complex regions and mapped their geology and composition in detail, and measured the topography of large, ancient impact features.

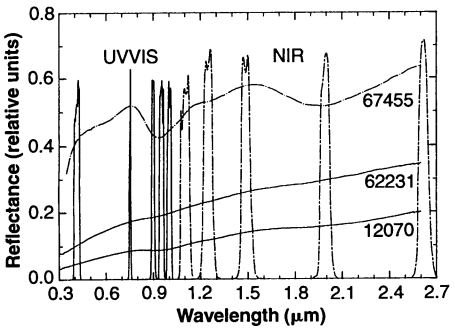

Fig. 3. Bandpasses of Clementine filters for the UVVIS and NIR cameras superimposed on reflectance spectra of lunar samples. In addition to these 10 filters, the UVVIS camera contained a broadband visible filter, and the NIR camera contained an additional filter centered near 2.8 μm. Sample 67455 is a feldspathic rock powder with low-calcium pyroxene from Apollo 16; sample 62231, an Apollo 16 soil, is also feldspathic, and the Apollo 12 soil (12070) is basaltic.

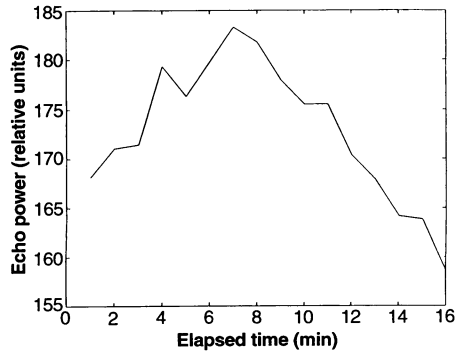

Fig. 4. Total power in right circularly polarized echoes versus time (t = 0 was 23:32:25 UTC). Minimum phase angle β_{min} occurs at the south pole near Δt = 13.5 min. If an icy deposit were offset from the pole toward Earth, the subtle peak might be shifted as shown.

The images from Clementine constitute the first global digital data set for the moon. The color of the moon in the visible to near-infrared part of the spectrum is sensitive to variations in both the composition of surface material and the amount of time the material has been exposed to space. The filters were selected to characterize the broad lunar continuum and sample parts of the spectrum known to contain absorption bands diagnostic of iron-bearing minerals and plagioclase feldspar, the dominant mineral constituents of the lunar crust (Fig. 3). By combining information obtained through several filters, we can use multispectral image data to map the distribution of rock and soil types on the moon.

Clementine successfully mapped the moon in 11 colors at an average surface resolution of about 200 m per picture element. Our initial examination of the data attests to its high quality. We have completed a preliminary look at the Clementine data on a global basis by reducing the resolution by a factor of several hundred, allowing the immense volume of data to be easily manipulated (*2*). Several major compositional provinces are evident, including the volcanic lavas of the maria (the dark regions of the moon), young craters, and the immense South Pole–Aitken Basin, a compositional anomaly on the far side of the moon (*2*). Preliminary studies of areas of already known geological complexity—including the Aristarchus crater and plateau (*3*), the Copernicus crater (on the western near side), and the crater Giordano Bruno on the eastern far side (*4*)—have allowed us to identify and map the diversity within and between geological units that have both impact and volcanic origins.

In addition to geological and compositional data from the images, Clementine has allowed us to see previously unknown regions of the moon and to see known areas from a different perspective. The science team completed a mosaic of the south polar region of the moon, using over 1500 UVVIS images, that reveals a previously unmapped portion of the moon near the pole. An extensive region of shadow corresponds to a large depression centered very near the south pole, possibly an ancient impact basin about 300 km in diameter (*5*). Its significance lies in its geographic position: Because the rotation axis of the moon is nearly perpendicular to its plane of orbit around the sun (axis inclination, 1.5°), much of this dark region near the pole may never receive sunlight. If so, it is very cold in these regions, possibly only about 40 K.

It has been suggested (*6*) that water molecules, added to the moon by impacting comets, may find their way into these "cold traps" and, over billions of years, accumulate in significant amounts. Clementine beamed radio waves into the polar areas, and the scattered radio signals were received on the large antennas of NASA's Deep Space Network. This "bistatic radar" experiment was designed to look for echoes that are diagnostic of water ice deposits. We expect that ice on the moon, if it exists at all, is limited in extent and is perhaps mixed with or buried under rocky material. The distinguishing radar characteristics will be muted. The echo might be only marginally stronger from icy regions, the peak might be subtle or broad because the ice may be distributed around the polar area, and only a change in polarization relative to nearby parts of the moon might be noticed. Relative echo power for one pass over the south pole is illustrated in Fig. 4. A small increase in echo strength was observed a few minutes before echoes would be received at the minimum phase angle for the south pole. This increase is accompanied by a small change in the polarization ratio. These observations are consistent with some ice being present, but displaced from the pole toward Earth. Many other (non-ice) explanations could also account for these results. Further calibration needs to be applied, and data from three other orbits with similar observing geometries will be analyzed.

The laser-ranging data from Clementine have allowed us to see the large-scale topography (or relief) of the lunar surface on a nearly global basis (−75° to +75° latitude). About 19% of the outgoing laser pulses were recovered. A striking result from this experiment is the confirmation of the existence of a population of very ancient impact basins whose outlines have been nearly obliterated by later impacts (*7*). The largest confirmed basin on the moon is 2500 km in diameter and over 12 km deep, making it the largest, deepest impact crater known in the solar system (*7*, *8*). Gravity data obtained from radio tracking of Clementine indicate that these great holes in the moon's crust are compensated to varying extents by plugs of dense rocks far below the surface; these dense plugs are probably produced by structural uplift of the mantle (the iron- and magnesium-rich layer below the low-density, aluminum-rich crust) beneath these impact basins (*8*). A global map of the thickness of the lunar crust has been derived from the combined analysis of the topography and the gravity field (*8*).

Detailed discussions of selected scientific topics are presented in the reports that follow this overview. Noteworthy observations not covered in these reports are briefly described below. The Clementine

mission enabled the first quantitative observations of the moon at very small solar phase angles. The moon exhibits a nonlinear increase in brightness as its face becomes fully illuminated to a terrestrial observer. The canonical explanation of this "opposition effect" is the rapid disappearance of mutual shadows cast by particles in the lunar regolith. Observations at small solar phase angles were important to obtain because models of the opposition effect are sensitive indicators of surficial compaction state and particle size (9). A recent model for optical coherent backscatter seeks to explain a narrow opposition spike at very small phase angles (<1°) seen on the Galilean satellites and by laboratory measurements of lunar samples (*10*, *11*). The Earth's finite angular size as seen from the moon precludes the measurement of the solar phase curve below ~0.5°; at this point, a lunar eclipse occurs. The Clementine spacecraft was able to obtain a large number of observations below 1°, including dozens at 0° phase. A solar phase curve based on a preliminary analysis of these images (along with some obtained at higher phase angles) (Fig. 5) shows a huge opposition surge on the moon, including a nearly 20% increase in brightness in the last 0.25°. This is comparable to the sharply peaked opposition spike observed on the bright icy satellite Europa (*12*), which has been attributed to coherent backscatter. No color dependence was detected in the lunar phase curve below 2°.

The LWIR camera imaged the daytime thermal-infrared emission in a bandpass centered at 8.75 μm (*13*). While nighttime temperatures are determined predominantly by the surface thermal inertia, daytime temperatures are controlled by the albedo and the surface roughness (*13*). The strong dependence on local topography can be seen in Fig. 6, which compares images of the crater Tycho obtained by the UVVIS and the LWIR cameras. Brightness temperatures were calculated with the Planck function for emission from a blackbody assuming unit emissivity; brightness temperatures range from a high of about 380 K on the equator-facing interior southern rim to a low of about 270 K on the southward-facing interior northern rim. The distribution of data number (DN) values is shown in Fig. 7. The presence of such a large spread of surface temperatures has important implications for understanding the surface temperature variation.

Radiative cooling to space will be different from that assumed in the common thermal models (which assume a flat surface); this is due to both the topographic influence, which results in thermal emission from one surface being absorbed by another surface rather than lost to space, and by the nonlinear thermal-emission dependence on temperature as T^4. As a result, interpretation of nighttime and eclipse surface temperatures (*14*, *15*) in terms of surface properties based on such models will be in error. Second, the nonlinear dependence of the emitted flux on temperature and wavelength will produce a gradient of derived brightness temperature with wavelength, with values at shorter wavelengths being greater than values at longer wavelengths. This will affect our understanding of composition derived from midinfrared spectroscopy (*16*). Although this effect has been described previously (*17*), the model used included only small-scale roughness and was somewhat unphysical. The actual spread of surface temperatures also should

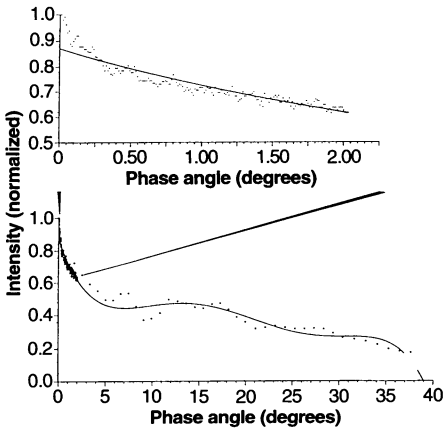

Fig. 5. The lunar solar phase curve based on Clementine images. The observations were obtained with the UVVIS camera at a wavelength of 0.9 μm. Preliminary calibrations and pointing information have been used. For phase angles below 2° (top), measurements were extracted from a single image. For larger phase angles (bottom), averaged values from individual frames were used. Limb darkening has been corrected with a Lommel-Seeliger photometric function. The solid line is a fifth-order polynomial fit.

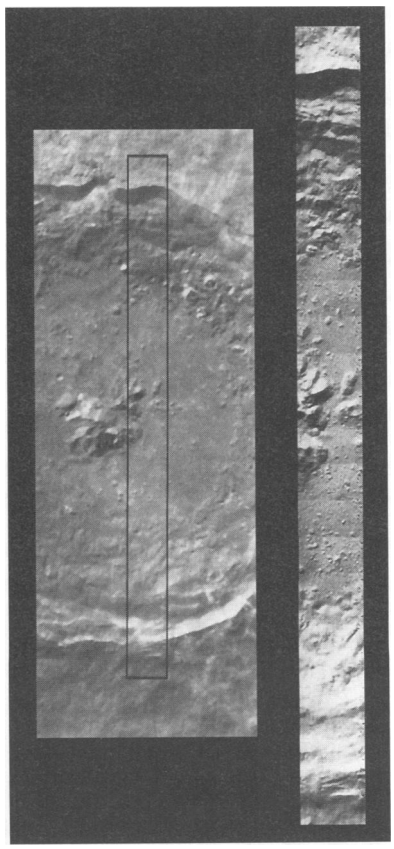

Fig. 6. UVVIS mosaic of the crater Tycho (left) and LWIR mosaic through the center of the crater (right). The box outlined on the UVVIS image shows the location of the LWIR data.

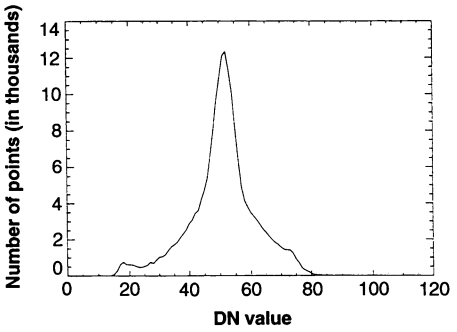

Fig. 7. Distribution of data number (DN) values in the LWIR mosaic shown in Fig. 6.

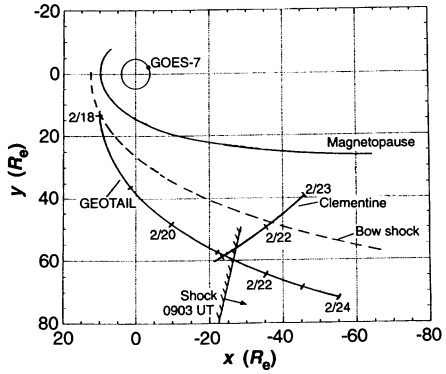

Fig. 8. A summary of spacecraft positions and the interplanetary shock wave passage during the solar energetic particle event of February 1994. The Clementine spacecraft was in lunar orbit at this time, and the orbit projection on the geocentric solar ecliptic (gse) *xy* plane is shown for 21 and 22 February 1994 (R_e, radius of the Earth). The GEOTAIL orbit is shown for 18 to 24 February. The GOES-7 spacecraft at geostationary orbit is shown for the particular position at 0900 UT on 21 February. The nominal magnetopause and bow shock surfaces are also shown in this projection. At 0903 UT, both Clementine and GEOTAIL saw a strong interplanetary shock wave pass over them, allowing precise orientation determination. GOES-7 (and also SAMPEX) in lower Earth orbit saw evidence of the shock passage more than 7 min earlier than Clementine.

include the effects described here that are attributable to the large-scale surface topography. Quantitative analysis of the Clementine thermal infrared imaging experiment can begin once the instrument calibration to radiance is completed. Incorporation of Apollo 17 infrared observations (*18*) will allow interpretation of surface physical properties at selected locations.

An important objective of the Clementine program was to investigate the effects of the space radiation environment on the advanced technologies and lightweight spacecraft components being flight-tested on board the Clementine spacecraft and the Interstage Adapter satellite. A charged particle telescope (CPT) was built, tested, and integrated on board the main Clementine spacecraft to measure the fluxes of energetic electrons and protons encountered by the spacecraft throughout its mission. The low-energy electron channels (25 to 500 keV) have provided extensive data on the interaction between the moon and the Earth's magnetotail: While orbiting the moon, the CPT saw the wake created by the moon when it blocked the flow of energetic particles along magnetotail field lines. The CPT has also observed numerous bursts of energetic electrons during geomagnetic storms and magnetospheric substorms. A particularly important goal of the CPT was to measure fluxes of energetic protons in the energy range 3 to 80 MeV, which are emitted during solar energetic particle events. A strong solar particle event was observed on 20 to 25 February 1994 and was associated with a very strong interplanetary shock wave passage at ~0900 UT on 21 February. The Clementine CPT observed this particle event and detected the precise time and position of the shock passage. The Clementine data were particularly valuable because they were obtained concurrently with measurements from several other near-Earth spacecraft (GOES-7, SAMPEX, GEOTAIL), thus permitting a remarkable multipoint study of the shock interaction with geospace (Fig. 8).

REFERENCES AND NOTES

1. A computer with a capacity of 1.7 million instructions per second (MIPS) used for safemode, attitude control, and housekeeping. A reduced-instruction set computer (RISC) 32-bit processor operating at 18 MIPS was used for image processing and autonomous operations. Also incorporated is a state-of-the-art image compression system provided by the French Space Agency (CNES). A data handling unit with its own microcontroller sequenced the cameras, operated the image compression system, and directed the data flow. During imaging operations, the data were stored in a 3-kg, 2-gigabit dynamic solid-state data recorder and later transferred to the ground stations using a downlink operating at 128 kilobits (kb) per second. The spacecraft was commanded by a 1-kb/s uplink from the NASA Deep Space Network and Department of Defense stations. Demonstration of autonomous navigation, including autonomous orbit determination, was a major goal of the Clementine mission. Autonomous operations were conducted in lunar orbit. Data compression was done on board by the CNES compression chip. This processing was performed on a completed, framed image before storage on the solid-state data recorder when the appropriate compression flag was set. The compression chip, developed by Matra Marconi (location) under CNES specifications, could be used in two modes, selectable by an uplink command. The first optimized root-mean-square error (for a nominal compression). The second mode (JPEG) provided visual optimization at a fixed compression rate. In the first mode, blocks of 8 by 8 pixel 8-bit data are transformed to a best-fit cosine series expansion in the orthogonal row and column directions. This algorithm tends to preserve high-frequency information with less loss than does JPEG at the same compression ratio. The nominal amount of compression was set by limiting the scene error induced by compression to a fraction of the camera's temporal noises. Analysis of lunar images during the first part of the mission showed that the quantitization matrix used by the chip was optimum for the imaging cameras. The HIRES camera was operated in JPEG mode. The high-frequency information in the HIRES scenes was spurious (it was caused by nonuniformity of the gain of the intensifier tube); eliminating high-frequency content allowed higher compression without harming the information content of the scenes. The average compression rate for all images obtained during the mission was 5.5.
2. P. G. Lucey *et al.*, *Science* **266**, 1855 (1994).
3. A. S. McEwen *et al.*, *ibid.*, p. 1858.
4. C. M. Pieters *et al.*, *ibid.*, p. 1844.
5. E. M. Shoemaker *et al.*, *ibid.*, p. 1851.
6. K. Watson, B. C. Murray, H. Brown, *J. Geophys. Res.* **66**, 3033 (1961); J. R. Arnold, *ibid.* **84**, 5659 (1979); A. P. Ingersoll, T. Svitek, B. C. Murray, *Icarus* **100**, 40 (1992).
7. P. D. Spudis *et al.*, *Science* **266**, 1848 (1994).
8. M. T. Zuber *et al.*, *ibid.*, p. 1839.
9. B. W. Hapke, *Icarus* **67**, 246 (1986).
10. _____, *ibid.* **88**, 407 (1990).
11. _____, R. M. Nelson, W. D. Smythe, *Science* **260**, 509 (1993).
12. D. L. Domingue, B. W. Hapke, G. W. Lockwood, D. T. Thompson, *Icarus* **90**, 30 (1991).
13. Precision is about 1 K at a surface brightness temperature of 400 K, 2 K at 300 K, and 10 K at 210 K. The DN correspondence is 100 DN to about 400 K, 25 DN to 300 K, and 2 DN to 200 K.
14. D. F. Winter, *Radio Sci.* **2**, 229 (1970); J. M. Saari and R. W. Shorthill, *Moon* **5**, 161 (1972); R. W. Shorthill, in *Thermal Characteristics of the Moon*, J. W. Lucas, Ed. (MIT Press, Cambridge, MA, 1972), pp. 3–50.
15. A. E. Wechsler, P. E. Glaser, J. A. Fountain, in *Thermal Characteristics of the Moon*, J. W. Lucas, Ed. (MIT Press, Cambridge, MA, 1972), pp. 215–242; B. M. Jakosky, in preparation.
16. P. G. Lucey, *Proc. Lunar Planet. Sci. Conf.* **21**, 417 (1991); D. B. Nash *et al.*, *J. Geophys. Res.* **98**, 23535 (1993).
17. P. E. Johnson, K. J. Vogler, J. P. Gardner, *J. Geophys. Res.* **98**, 20825 (1993); K. V. Vogler, P. E. Johnson, R. W. Shorthill, *Icarus* **92**, 80 (1991).
18. W. W. Mendell and F. J. Low, *Moon* **9**, 97 (1974).
19. The LWIR images had a space background subtracted and had hot pixels removed by means of a median filter. A flat field shows variations in pixel sensitivity that are much smaller than the observed geographic variation; the flat-field variation has not been corrected.

16 September 1994; accepted 15 November 1994

The Shape and Internal Structure of the Moon from the Clementine Mission

Maria T. Zuber,* David E. Smith, Frank G. Lemoine, Gregory A. Neumann

Global topographic and gravitational field models derived from data collected by the Clementine spacecraft reveal a new picture of the shape and internal structure of the moon. The moon exhibits a 16-kilometer range of elevation, with the greatest topographic excursions occurring on the far side. Lunar highlands are in a state of near-isostatic compensation, whereas impact basins display a wide range of compensation states that do not correlate simply with basin size or age. A global crustal thickness map reveals crustal thinning under all resolvable lunar basins. The results indicate that the structure and thermal history of the moon are more complex than was previously believed.

Though formed in the same part of the solar system, the Earth and moon have followed dramatically different evolutionary paths in their 4.6-billion-year histories. Absolute ages of the lunar surface revealed by the Apollo missions (*1*) demonstrate that volcanism and tectonism indicative of substantial heat loss from the lunar interior essentially ceased by 2.5 to 3 billion years ago, in contrast to Earth, which remains geologically active to the present day. The fundamental difference in thermal evolution between the Earth and moon has typically been attributed to the planets' different size and mass (*2*)—the moon contained fewer radiogenic heat-producing elements because of its smaller volume and cooled faster because of its higher surface area-to-volume ratio as compared with Earth. Beyond this basic knowledge, however, understanding of the thermomechanical evolution of the moon has been elusive, largely because of limited knowledge of lunar internal structure.

The Clementine mission, sponsored by the Ballistic Missile Defense Organization, with participation from NASA, mapped the moon from late February through early May 1994 (*3*). Included in the spacecraft instrument complement were a laser ranging device and an S-band microwave transponder from which topographic and grav-